Ocean Dynamics (2014) 64:833–846
DOI 10.1007/s10236-014-0711-z

On the developments of spectral wave models: numerics and parameterizations for the coastal ocean

Aron Roland · Fabrice Ardhuin

Received: 13 September 2013 / Accepted: 6 March 2014 / Published online: 21 May 2014

Abstract The development of numerical wave models for coastal applications, including coupling with ocean circulation models, has spurred an ongoing effort on theoretical foundations, numerical techniques, and physical parameterizations. Some important aspects of this effort are reviewed here, and results are shown in the case of the French Atlantic and Channel coast using version 4.18 of the WAVEWATCH III^R model. Compared to previous results, the model errors have been strongly reduced thanks to, among other things, the introduction of currents, coastal reflection, and bottom sediment types. This last item is described here for the first time, allowing unprecedented accuracy at some sites along the French Atlantic Coast. The adequate resolution, necessary to represent strong gradients in tidal currents, was made possible by the efficiency brought by unstructured grids. A further increase in resolution, necessary to resolve surf zones and still cover vast regions,will require further developments in numerical methods.

Responsible Editor: Bruno Castelle

This article is part of the Topical Collection on the *7th International Conference on Coastal Dynamics in Arcachon, France 24–28 June 2013*

A. Roland
Institut für Wasserbau und Wasserwirtschaft, Technische Universität Darmstadt, Darmstadt, Germany

F. Ardhuin (✉)
Laboratoire d'Oceanographie Spatiale, Ifremer, Plouzan, France
e-mail: ardhuin@ifremer.fr

Keywords Wave modeling · Bottom friction · Coupling · Wave-current interaction

1 Introduction

The first spectral numerical wave model was developed in the 1950s to deal with dispersive swell propagation arriving in Morocco. This approach was soon generalized and led to the development of a succession of numerical wave models (SWAMP Group 1984; Komen et al. 1994). So what does it take to make an accurate wave model, and how accurate can be the wave hindcasts in coastal waters? Seven years after the publication of a collective review on numerical wave modeling (WISE Group 2007), the present paper aims at providing some updates on specific issues, in particular, numerical methods and bottom friction. In adapting our paper from the Coastal Dynamics Conference (Ardhuin and Roland 2013), we have left out theoretical aspects related to wave-current interactions and corrected a few errors.

We focus on numerical wave models in Section 2, with an application to the French Coast in Section 3 , followed by perspectives, outlined in Section 4. Driven by this application, the present paper is not a full review of a very extensive literature nor a specific study of a single particular problem. Instead, it touches on several practical issues and attempts to link them to more fundamental problems. Our point of view is centered on the WAVEWATCH III modeling framework (Tolman 2009) and more specifically its application with triangle-based meshes. Still, many aspects discussed below are also relevant to other numerical wave models.

2 Spectral wave models: inherent limitations and recent progress

2.1 Waves, statistics, and spectra

The basic idea of spectral wave modeling is to represent the random nature of the sea surface elevation by its generalized Fourier spectrum, evolving slowly in space and time (Priestley 1965). Some available spectral models include the phase information, which provides information on wave asymmetry and skewness (Herbers and Burton 1997). This information is particularly relevant in shallow water, but these models have not been widely adopted by the research or engineering community probably because of the conceptual difficulty of working with both spectra and bi-spectra. Outside of the surf zone, phase-resolving models have been used very successfully in ocean engineering applications, when the details of the wave shape and flow are required (e.g., Dommermuth and Yue 1987) and also to verify the underlying hypotheses of phase-averaged model and their statistical closure (Tanaka M 2001).

However, in this region of the ocean, it was found repeatedly by Tayfun (1980) and Fedele and Tayfun (2007) that the full statistics of the sea surface are very well described by the quasi-linear random wave model: waves can be represented as a superposition of wave trains that are locally sinusoidal and that propagate in all possible directions with all possible frequencies, with an intrinsic period $T = 1/f = 2\pi/\sigma$ and wavelength $L = 2\pi/k$ related by the linear dispersion relation for free surface gravity waves $\sigma^2 = gk\tanh(kD)$ as a function of the local mean water depth D (de Laplace 1776). The intrinsic frequency f is the frequency of waves in the frame of reference moving with the local horizontal "current." As a result, the general three-dimensional wave spectrum collapses to a two-dimensional spectrum and the phases are essentially random and do not require any particular attention. One only needs to focus on one scalar, the spectral density of sea surface elevation (usually called energy). This scalar is a function of two spectral dimensions that is usually chosen among the pairs wavenumber and direction (k, θ), frequency and alongshore wavenumber (f, k_y), or more usually, intrinsic frequency f and direction toward which waves are propagating, θ, as shown in Fig. 1. From this surface elevation spectrum, it is possible to compute the spectra, and thus the full statistics of any other wave-related parameter such as velocities, pressure, and surface slopes.

For extreme events, including the famous "freak waves," a second-order correction estimated from the wave spectrum is enough to explain the statistics of extremes and correct the wave spectrum for the presence of lowest-order bound wave components (Tayfun 1980; Janssen 2009). This correction can also be used to estimate the skewness of the sea surface, a property related to the sea state bias in satellite altimetry (e.g., Elfouhaily et al. 1999). This second-order correction also includes the partial standing wave term that makes it possible to measure waves without getting wet, using seismic stations on land (see Ardhuin and Herbers 2013 for a review of the theory) or acoustic records at large depths (Farrell and Munk 2008; Ardhuin et al. 2013). There are thus many good reasons to use spectral wave models for the estimation of the second-order spectrum. Because this second-order spectrum is a function of the full directional (first order) wave spectrum, the measurable second-order

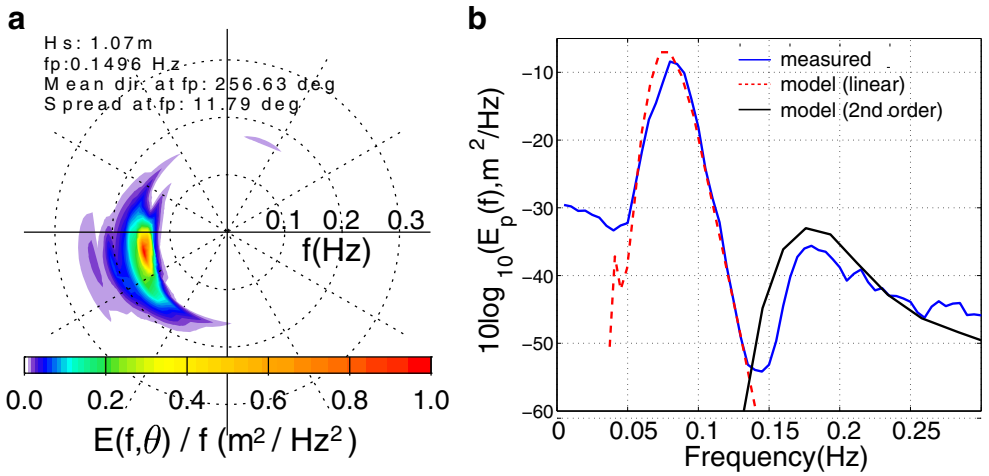

Fig. 1 Two examples of wave spectra. **a** Obtained from a stereo-video system measuring maps of sea surface elevation (Benetazzo 2006) deployed on the Katsiveli platform near Sevastopol, Ukraine and **b** spectrum of bottom pressure from a SBE26 tide gauge deployed in 100-m depth offshore of Brest compared to its simulation from global wind fields using the WW3 code. The measured spectrum is compared to a numerical model result for both the linear part and the second-order correction (Ardhuin et al. 2013). In this case, this second-order contribution is the reason why it is impossible to estimate the spectrum for waves with frequencies above 0.13 Hz

properties can also be used to validate the shape of the first order spectrum produced by models. Indeed, the full spectrum is almost never available in enough details, except when using dense arrays or techniques such as stereo-video imagery, as illustrated in Fig. 1.

Wave buoys or colocated combinations of pressure and velocity measurements only provide five parameters for each frequency. The validation of the second-order spectrum estimated from a modeled directional spectrum thus provide more information on the width of the peak in the case of subharmonics and on the presence of partial standing waves in the case of the super-harmonics, such as induced by partial reflection (e.g., Touboul and Rey 2012). However, this second-order theory is only valid for a flat bottom and breaks down in shallow water, where it fails to represent the net transfer of energy to free components with shorter periods (super-harmonics) or very long periods (subharmonics also known as infragravity waves). A proper representation of these effects requires the use of a bi-spectrum that carries the relative phase information of the different wave components (e.g., Herbers and Burton 1997). Several parameterizations have been proposed with some success (Becq-Girard 1999; Toledo et al. 2012), avoiding the higher computational cost incurred when computing the bi-spectrum evolution. These triad nonlinear effects may also be ignored, and accurate significant wave heights can still be obtained (e.g., Thornton and Guza 1983 and Filipot and Ardhuin 2012), but the the shape of the wave spectrum will not contain the harmonics that have been liberated during propagation over varying topography or currents. We will now focus on the ocean outside of the surf zone.

2.2 Theoretical bases of the wave action equation

Over the last 20 years, models based on the spectral wave action equation (WAE) such as the WAM (WAMDI Group 1988), TOMAWAC (Benoit 1996), SWAN (Booij 1999), and WW3 (Tolman 2002b) have gained widespread usage thanks to the versatility of the WAE for including various sources and sinks of energy.

The WAE gives the evolution in space and time of the wave spectrum, represented by the action spectral densities. Assuming linear and irrotational wave theory, it is

$$A(k,\theta) = \frac{E(k,\theta)}{\sigma} = \frac{E(f,\theta)}{2\pi C_{\mathrm{g}}(f,D)\sigma} \tag{1}$$

where σ is the relative radian frequency. The most general form, given by Andrews and McIntyre (1978), is valid for nonlinear and rotational waves, with an intermediate approximation in (Willebrand 1975). $C_{\mathrm{g}}(f,D)$ is the group velocity, which for linear waves is only a function of the intrinsic frequency f and water depth D. The wave action is advected at a velocity given by the intrinsic group speed vector $\mathbf{C}_{\mathrm{g}}(f,D)$, which has a norm equal to $C_{\mathrm{g}}(f,D)$ and a direction θ, plus an advective current velocity vector $\mathbf{U}_A(f,\theta)$ which is the generalized Lagrangian mean velocity (Andrews and McIntyre 1978). So far, the public versions of numerical models such as SWAN or WW3 do not bother with this kind of detail and use instead the same surface current velocity vector $\mathbf{U}$ for all spectral components instead of a more general $\mathbf{U}_A(f,\theta)$. For slowly varying depths and currents, the WAE takes the following form,

$$\frac{\partial A(k,\theta)}{\partial t} + \nabla_x \left[\left(\mathbf{C}_{\mathrm{g}}(k,\theta)+\mathbf{U}\right) A(k,\theta)\right] + \frac{\partial}{\partial k}\dot{k}A(k,\theta) + \frac{\partial}{\partial \theta}\dot{\theta}A(k,\theta) = \frac{S_{\mathrm{tot}}(k,\theta)}{\sigma}, \tag{2}$$

where S_{tot} is the "total" energy source term, involving all processes that contribute to the change of wave energy, except for the adiabatic exchange of energy with varying currents (Phillips 1977). The WAE is written here on a flat surface and is easily generalized to the curved ocean surface.

The evolution of the action spectrum is further modified by source terms that represent a wide range of processes, including generation by the wind, nonlinear evolution of the waves, dissipation by breaking, dissipation by friction at the air-sea interface, and bottom friction. Each of these source terms is computed from theoretical bases and empirical adjustments.

Finally, wave propagation can be improved compared to the usual linear waves and geometrical optics approximations. Holthuijsen et al. (2003) and Liau et al. (2011) have reproduced some of the diffraction effects that occur in cases where interference from distinct diffraction centers can be neglected, but the full effect of diffraction cannot be reproduced in phase-averaged models. Another regime that is appropriately handled with the WAE is the scattering of waves by random current or depth perturbations (Rayevskiy 1983; Ardhuin and Magne 2007). A generalized WAE that takes into account higher order effects of current and depth gradients has been proposed by Toledo et al. (2012), but it has not yet been implemented into numerical wave prediction models. It should be noted that on natural topographies, even in the presence of very large gradients in the wave field, the effect of diffraction is generally limited (Magne et al. 2007).

2.3 Numerical integration of the wave action equation

Without the source terms, the conservative WAE could be solved exactly by a Lagrangian approach, using ray-tracing methods, with a most practical integration using backward ray tracing (O'Reilly and Guza 1991). Introducing source terms in ray tracing makes the solution method difficult,

in particular, if the rays move with time due to changing water levels or currents (Ardhuin et al. 2001). This is simplified by integrating rays over a single time step, as done in the TOMAWAC model (Benoit 1996), but at the price of some diffusion due to interpolation which may still be much less than the diffusion with a first-order finite difference scheme that may be use in other types of models like SWAN or WW3 (Ardhuin and Herbers 2005). Instead, the unsteady four-dimensional problem can be formulated in a Eulerian way, as in Eq. 2. The left-hand side of that equation can be integrated with common numerical schemes such as finite element methods, finite volume methods, finite difference methods, or residual distribution schemes on either structured or unstructured grids using various time stepping strategies as done in WAM, WW3, SWAN, and other models (Roland 2008). Recent numerical developments have largely focused on the improvement of methods on unstructured grids made of triangular meshes (e.g., Roland 2008 and Zijlema 2010), the use of quadrangles with variable sizes (Popinet et al. 2010; Li 2010), or grid nesting (Tolman 2008). The variability of the grid resolution across the domain exacerbates the problems outlined above.

The solution strategies in these models use either the fractional step method of Yanenko (1971) or solve the problem directly, using implicit time stepping techniques proposed by Patankar (1980). The latter methods form the basis of the SWAN model (Booij 1999) and are very efficient in steady conditions because they do not have a strict Courant-Friedrichs-Levy (CFL)-like stability criterion, thus allowing very large time steps. When using large time steps, the solutions are not necessarily accurate.

2.3.1 Wave propagation

The implicit method in SWAN leads to unphysical solutions when waves are strongly refracted over steep slopes (Gonzalez-Lopez et al. 2011), and certain limiters in spectral space must be applied as outlined in Dietrich et al. (2013). In that paper, it is mentioned that the turning of the certain wave component within one time step must remain in the quadrant of the current "sweep." In practice, it should be less than one spectral increment, and similar constraints apply to frequency space when waves go over strong current gradients. The realistic applications with the unstructured version of SWAN (Zijlema 2010) were obtained by setting the refraction term to zero in shallow water (Dietrich et al. 2011), which is the strongest possible limiter.

The effect of the Dietrich et al. (2013) limiter is evaluated by running the SWAN model on a structured grid using the first-order (BSBT; Booij 1999) and higher-order schemes (SORDUP; Rogers 2002), with and without the limiter. Here, we only show results for the laboratory case of a shoal over a sloping bottom (Vincent and Briggs 1989). The water

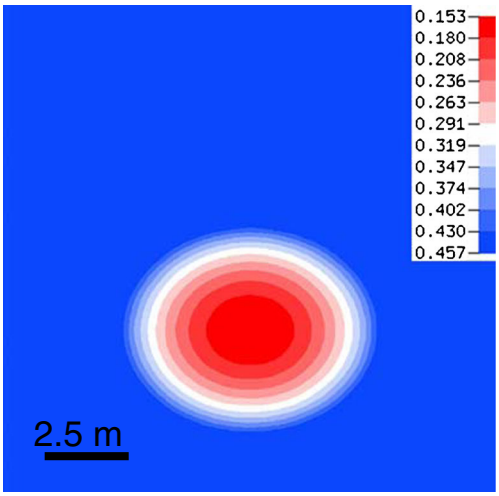

Fig. 2 Depths for the elliptic shoal case at the laboratory scale of Vincent and Briggs (1989)

depths are displayed on Fig. 2. Similar behavior was found for realistic cases. Figure 3 shows results of these runs. The incoming waves have a period of 1.305 s and a wave height of 5.5 cm. The spatial resolution is 0.2 m for the structured mesh, and we used one frequency bin and 240 directional increments in order to represent a monochromatic wave train. This directional resolution is intermediate between the 24 or 36 directions used in most practical application and the 3,600 directions used to verify model refraction properties (Ris et al. 2002). With a time step $dt = 0.11$ s that gives a CFL number of 1 for spatial advection, this large number of directions gives a similar CFL for the direction space, here up to 0.49.

For this case, depending on the order of the scheme, the influence of these limiters may be up to 50 % variation of H_s, the significant wave height. In particular, the wave height with limiter is lower in the focusing region. Similar differences occur in realistic cases. Looking at the case of the Haringvliet Estuary (Ris et al. 1999; Zijlema 2010), the limiter results in wave height differences up to 20 % with, again, a reduction in the maximum wave heights. As a result, although the limiter may guarantee a reasonable model result, removing very large wave spurious heights in the presence of steep slopes, it has a clear impact on the solution.

Another particular issue with the implicit methods, comes from the Godunov order barrier theorem (Godunov 1954). Namely, schemes more accurate than first order must either be nonlinear, and very difficult to integrate numerically, or non-monotone. Non-monotone means that in the vicinity of strong gradients, these schemes produce spurious oscillations possibly leading to negative wave energies. This unphysical result can be eliminated by setting negative values to zero, but the scheme loses its conservative

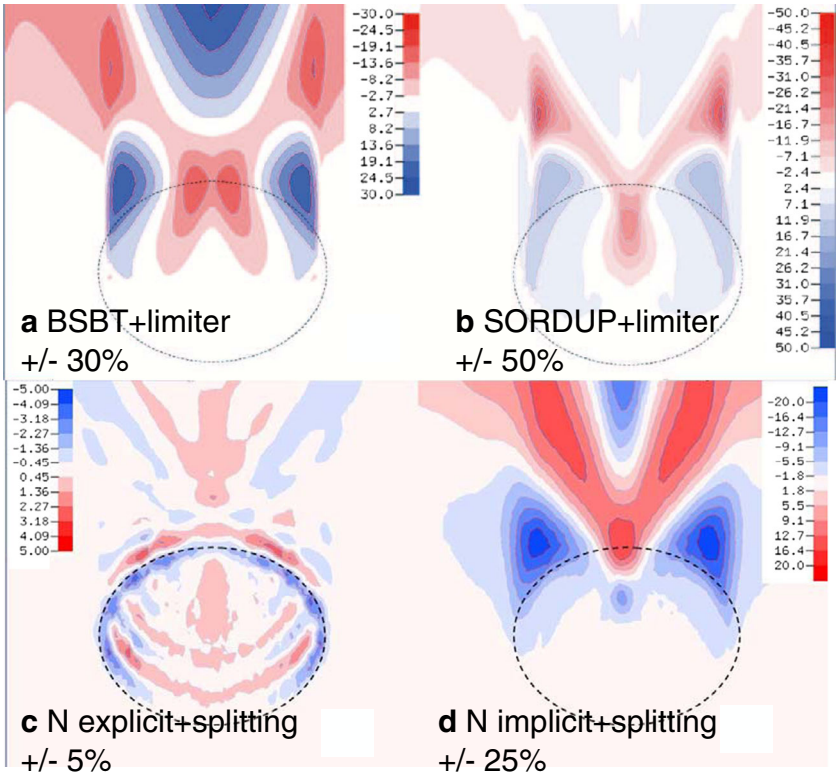

Fig. 3 Impact of numerical schemes on wave heights over the elliptic shoal, illustrated by differences in wave height (in percent). Effect of refraction limiter in the SWAN model with **a** first order BSBT scheme and **b** second-order scheme; the *colors* show the difference between simulations with and without limiter. Effect of splitting errors in WWM-II with **c** an explicit N-scheme and **d** the implicit N-scheme; the *colors* show the difference between large and small time steps, with ten sub-cycles for the large time step

properties. In SWAN's, when the SORDUP scheme is used, a "renormalization" of these negative energies was introduced, smoothing them out in the directional space while keeping the gradients in the physical space. This introduces strong numerical dispersion. This issue is especially visible when looking at parameters such as directional spread, which is already affected by numerical diffusion. In these cases, the higher-order schemes do not converge to the analytical solution when spectral and spatial resolution is increased (Ardhuin and Herbers 2005; Roland 2008).

In contrast, fractional step (splitting) methods separate the WAE integration into an ordinary differential equation for the source term integration and a hyperbolic partial differential equation for the propagation part. Once separated, specific numerical schemes and solution procedures can be applied most efficiently and accurately for each. This splitting technique gives excellent results in deep ocean and is used in combination with explicit time integration methods for the propagation part in codes such as WW3 or WAM, which are used by most weather forecasting centers. However, in shallow areas, where strong variations of depth and currents have a strong effect on wave propagation, the numerical efficiency of explicit methods is limited by the strict CFL criterion, which may require a very small stable time step for a stable solution. This drawback can be partly circumvented by splitting not only propagation and source terms but also spectral and geographical advection and introducing sub-cycling as done in WW3. Hence, the time step is only reduced for integrating one term in the WAE equation. In practice, the refraction is also limited in WW3, by the user-defined refraction time step, which was introduced for efficiency and better load-balancing on parallel computing systems. That limiter used to be applied on the depth-induced refraction only, it is now applied, since version 4.05 on the full refraction term, because currents in very shallow water can also lead to very large CFL numbers.

The splitting technique relaxes the time step constraint on the whole system, especially in the presence of steep bottom slopes: the relatively cheap refraction computation can be integrated with a very small step, while the spatial propagation is integrated with its own time step. Due to the sub-cycling, however, splitting errors are introduced into the solution. Namely, the solution of the split integration is not exactly equal to the solution of a single integration of the whole equation, and the difference grows with the number of sub-cycles (see, e.g., Roland 2008). When the surf zone needs to be resolved, or in some tidal channels, the model stability may require a very small time step. Here, implicit methods can be applied for geographical space advection to gain some efficiency, which is an option for unstructured grids in version 4 of WW3, but the splitting error remains.

In order to evaluate the error of splitting, we have run the Wind Wave Model-II (hereinafter WWM-II (Roland 2008)) for the same case, with the same physical and spectra resolutions. To quantify the splitting error, we have increased the global time step by a factor 10, to $dt_G = 1.1$ s, with a

time step of the sub-cycles kept at 0.11 s. The integration in directional space uses the ULTIMATE QUICKEST scheme (Leonard 1991) and spatial advection is performed by the N-Scheme as implemented in WWM-II and WW3 (Csík et al. 2002; Roland 2008). With the explicit version of the scheme scheme, the splitting errors does not exceed 5 %, whereas the implicit scheme produces errors greater than 20 % with a pattern that resembles the limiter effect in SWAN. Hence, limiters and splitting errors may result in large errors. The great benefit of splitting methods is that they converge to the true solution when the time step is reduced, which, in practice, may be very expensive in computation time. Explicit schemes produce smaller errors, which is due to the fact that gradients are well captured by the sub-cycling, whereas implicit schemes are more diffusive. The splitting error evaluated here is only due to the separate integration of spatial and spectral advection and does not exist with methods based on ray tracing. However, when source terms on the right-hand side of the WAE are strong, which is the case of wave breaking in shallow water, the splitting error may be even larger and all available methods struggle to solve the WAE efficiently and accurately.

2.3.2 Source terms

For the integration of these source terms, all spectral wave models apply an additional limiter, which is either linearized following the Patankar rules (see also Booij 1999) or integrated as an ODE (ordinary differential equations) problem within a separate fractional step. This limiter was introduced in the integration of the source terms (WAMDI Group 1988; Hersbach and Janssen 1999; Hargreaves and Annan 2000; Tolman 2002b). Within the splitting method, this limiter is only applied to the source term part when the ODE problem is solved. On the contrary, in direct methods (i.e., joint integration of both left and right-hand sides), the application of the limiter on the full integration, as done in the SWAN model, will limit the sum of all terms including propagation, which may have strong influence on the transient solutions in unsteady environments.

Selective computations of the various terms and limiters would be a pragmatic engineering solution to reduce the influence of limiters in certain regions and impose them in others where the solution is not of major concern. This may well make the schemes inconsistent and possibly not convergent (Lax and Richtmyer 1956). A similar problem was already corrected in SWAN (e.g., Zijlema and van der Westhuysen 2005).

For all these reasons, the solution of the WAE in inhomogeneous environments is a complex problem with many open challenges from the physical and numerical points of view. Dedicated numerical schemes must be investigated to arrive at efficient, stable, and accurate integration of wave evolution. The WAE equation can be integrated with higher-order implicit methods that are stable and monotone, but which must be nonlinear (Godunov 1954). Such methods, that can avoid splitting errors and effects of non-monotonicity, are under development and results will be reported elsewhere. The specific numerics of wave coupling to ocean circulation models (e.g., Dietrich et al. 2011 and Roland et al. 2012) is another area that will require special attention.

3 Application: from global to coastal wave modeling

3.1 Boundary conditions from global models

In general, the accuracy of wave model results in terms of significant wave height is governed in decreasing order of importance by

- the accuracy of forcing fields: first, the wind (and/or the offshore boundary in cases of nested grids), then the currents, and finally the water levels. This order is reversed where water depths limit the wave height because of breaking; there, the water level is the primary control on the sea state.
- the accuracy of source term parameterizations
- the effect numerical schemes.

This order is generally verified for large scales, and the developers of numerical wave models have found it convenient to blame the poor quality of atmospheric models for poor wave model performance, especially in coastal areas (e.g., Cavaleri and Bertotti 1997). Yet, the performance of operational atmospheric models is improving at a dramatic pace, with errors on wind speed reduced by more than 20 % between 1992 and 2006 (Janssen 2008). With these improvements, it has become increasingly clear that wave model parameterizations could be upgraded. Figure 4 shows the reduction in wave model errors on the significant wave height, when changing the wave generation and dissipation terms from the WAMDI Group (1988), to the ones by Tolman and Chalikov (1996), Bidlot (2005) and, possibly the most accurate formulation to date, the one by Ardhuin et al. (2010) with a recent update by Rascle and Ardhuin (2013). That parameterization was a compromise mostly suited to the global scale, and still suffers a weak growth bias at short fetch, which could be corrected by improving on the wind stress parameterization used in the wave generation term. As a result, modelers may prefer the parameterizations of van der Westhuysen et al. (2007) or Filipot and Ardhuin (2012) in enclosed areas. This was particularly well demonstrated by Alves et al. (2013) in the North American Great Lakes. Further progress is certainly on the way, with

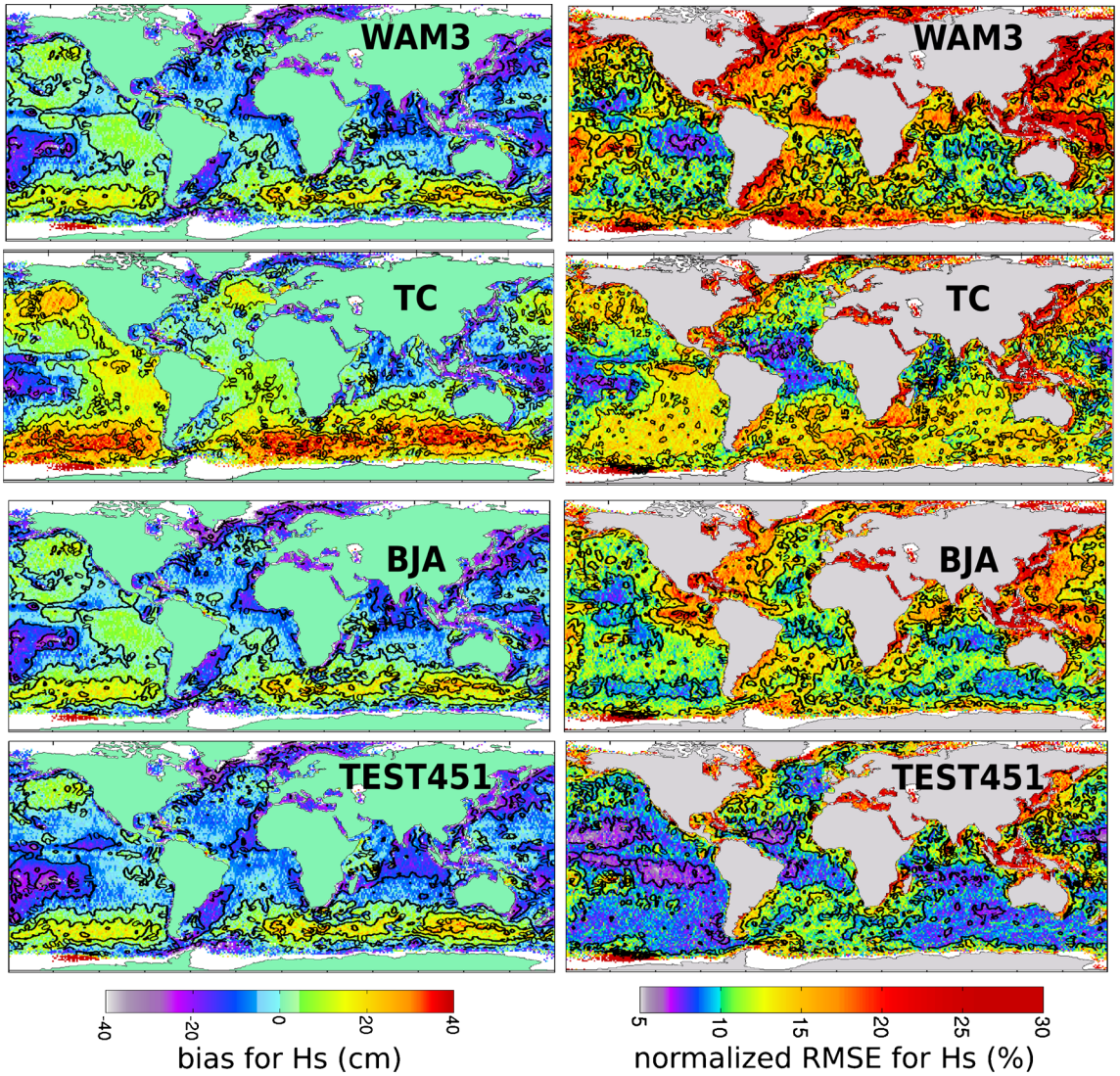

Fig. 4 Bias and normalized RMS error against altimeter data for the year 2007, using the same forcings but four different parameterizations of the wind input and dissipation: WAM Cycle 3 (WAMDI Group 1988), TC (Tolman and Chalikov 1996), BJA (Bidlot 2005), and TEST451 (Rascle and Ardhuin 2013). *Solid lines* in the right column correspond to contours at the 7.5, 10, 12.5, 15, and 20 % levels

ongoing research projects that are addressing the question of parameterizations (e.g., Tolman et al. 2013).

These improvements have further revealed flaws in the model forcing. In particular, the bands of low and high bias along the equatorial Pacific are clearly associated with ocean currents (Rascle et al. 2008), while icebergs in the southern ocean have been found to be a major source of error if not taken into account (Ardhuin et al. 2011). In the global results shown here, icebergs are represented, but the surface currents are still neglected due to large errors in global ocean circulation models.

The little impact of advanced numerical schemes on the model scores for the significant wave height H_s may be rather discouraging to model developers, but it comes from the smoothing effect of low-order schemes. Indeed, European Centre for Medium-Range Weather Forecasts (ECMWF) and Meteo-France still use first-order upwind scheme similar to the original WAM code (WAMDI Group 1988), which gives lower r.m.s. errors for H_s in most of the world ocean. However, the third-order scheme used here can give much better results when the wave field is partitioned into swells and wind seas and errors on swell heights are considered (Wingeart 2001). Such a scheme, however, requires a careful treatment of the spectral discretization in order to mitigate the "Garden Sprinkler Effect" that leads to a spatial discretization of the waves propagated from

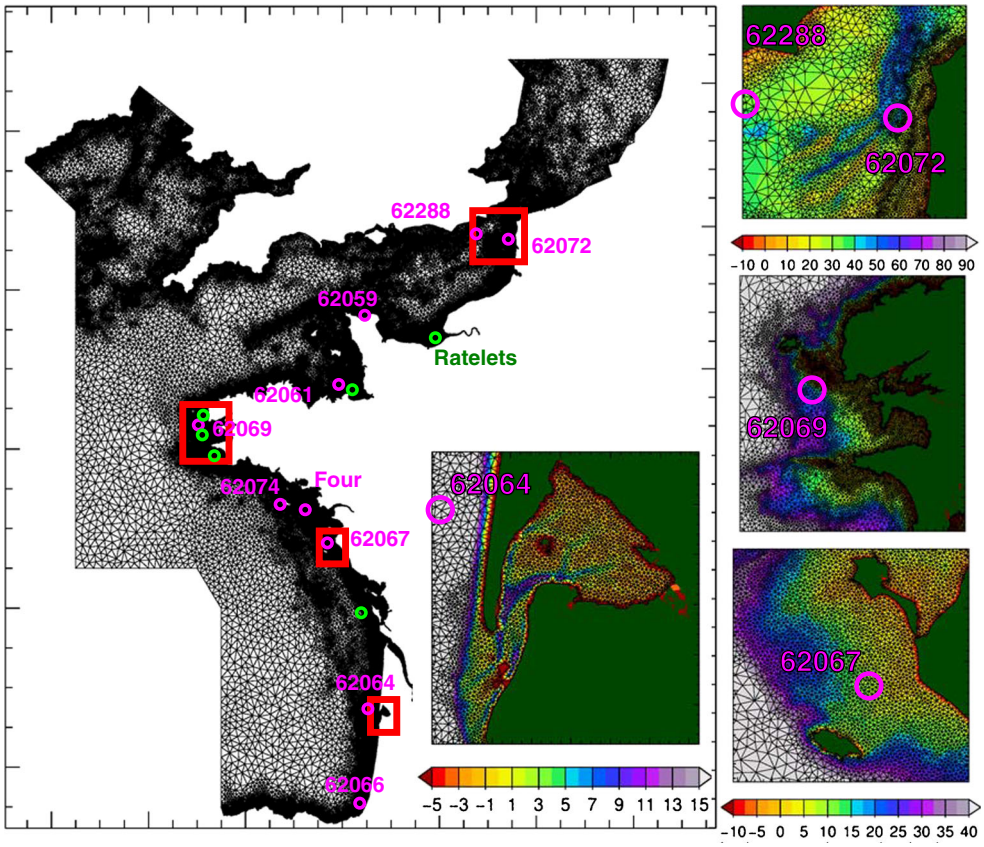

Fig. 5 Map showing the North Sea-Channel-Biscay mesh used for our hindcasts and forecasts. *Magenta* and *green circles* show location of permanent and temporary buoys used for calibration or validation in addition to satellite altimeter data. *Insets* are zooms of four grid areas, showing typical alongshore resolutions, with *color bars* displaying the elevation relative to mean sea level, in meters. The full mesh contains 110,000 wet nodes

a compact source because of the spectral discretization (Booij and Holthuijsen 1987; Tolman 2002a).

3.2 Coastal seas

When moving toward the coastal ocean, many effects can come into play. For open coasts, the quality of lateral boundary conditions from a global or regional wave model is obviously important because the waves mostly come from the open ocean. In the case of the French Atlantic Coast, the TEST451 parameterization (Ardhuin et al. 2010; Rascle and Ardhuin 2013) generally produces a 10 to 20 % excess of wave energy for wave periods between 12 and 16 s, especially on west coasts. For longer wave periods, up to 25 s, the global wind fields are very important. In particular, the ECMWF operational analysis systematically underestimate the highest winds that lead to these very long swells, whereas the CFS Reanalysis (Saha et al. 2010) and the NCEP operational analysis provide more consistent values in the high wind range. As a result, our hindcasts with ECMWF analyses lead to an underestimation of these long wave components because they are not properly generated in the deep ocean. For example, the Quirin storm with the highest ever measured sea state on February 15, 2011 (Hanafin et al. 2012) gave swell heights of 3.8 m at buoy 62074 when considering periods larger than 20 s, when these did not exceed 2 m in the model forced by ECMWF analyses.

Coastal areas are often influenced by strong currents, driven by either tides or water density gradients. Recent works have shown that wave model results can be strongly improved by taking into account currents, and their effects on wave refraction, enhanced wave breaking, and change in relative wind speeds (van der Westhuysen et al. 2012; Ardhuin et al. 2012). Another important effect, when the water depth is less than half the dominant wavelength, is the bottom friction. It has been known for decades that bottom friction may lead to strong wave energy dissipation (e.g., Shemdin 1980), reducing the wave height by as much as a factor 3 in some conditions (Ardhuin et al. 2003b). Still, a physically based parameterization of this effect had not been introduced into mainstream spectral wave models until now. Here, we particularly discuss the implementation in WW3 of the movable bed bottom friction proposed by Tolman (1994) and adjusted using data from the Shoaling Waves Experiment (SHOWEX; Ardhuin et al. 2003b).

3.3 The IOWAGA hindcast and Previmer forecasting system

Model implementation Based on the same WW3 code already used for the global ocean, we have used a 110,000 node unstructured mesh with an alongshore resolution of 300 to 500 m, shown in Fig. 5. This WW3 model configuration uses 32 frequencies from 0.037 to 0.72 Hz and 24 directions. It is forced at the boundary by the output of a multigrid WW3 system that combines 0.5 and 0.15° resolution grids for our region of interest (Rascle and Ardhuin 2013). The WAE is integrated in parts over 180 s steps. The spatial propagation part uses the N-scheme for the Csík et al. (2002) and Roland (2008), with a maximum time step of 60 s for the sub-cycles, dynamically adapted for each spectral component but always more than 15 s. The source terms are integrated with a variable time step that can be as low as 5 s. Most of the cost of the calculation lies with the advection.

This model is forced by operational ECMWF wind analysis at a resolution of 0.25° or better, with a time step of 6 h (3 h since January 2013, thanks to the combination of forecasts and analyses). Currents and water levels on a series of grids with a resolution of 200 m is provided by the Previmer system based on the MARS2D model. A map of median grain size has been established from the French Hydrographic Service (SHOM) database (Garlan 1995, 2009).

Model results can be viewed on the wave modeling page of http://www.previmer.org, with numerical results available at http://tinyurl.com/iowagaftp, including full spectra for over 4,000 grid points and the full frequency spectrum over the entire grid. At this spatial resolution, the refraction over shoals and tidal currents and the sheltering by islands and headlands are accurately represented (Ardhuin et al. 2013). The same model settings have been used with CFSR winds for a 20-year hindcast also available (Boudière et al. 2013).

Calibration and validation of bottom friction A preliminary analysis of all the available buoy data showed an anomalous behavior for the Yeu buoy (WMO number 62067), with measured wave energies much lower than predicted using the bottom friction parameterization loosely derived from the JONSWAP experiment (Hasselmann et al. 1973; Bouws and Komen 1983) or the SHOWEX movable bed friction using medium sand grain sizes (Ardhuin et al. 2003a). These measurements are also confirmed by the few good data, between Yeu Island and the mainland, from the Jason-1 altimeter track. In fact, an inspection of the sediment cover reveals that the buoy lies down-wave of a 20 km-wide region of shallow rock platforms (Fig. 6).

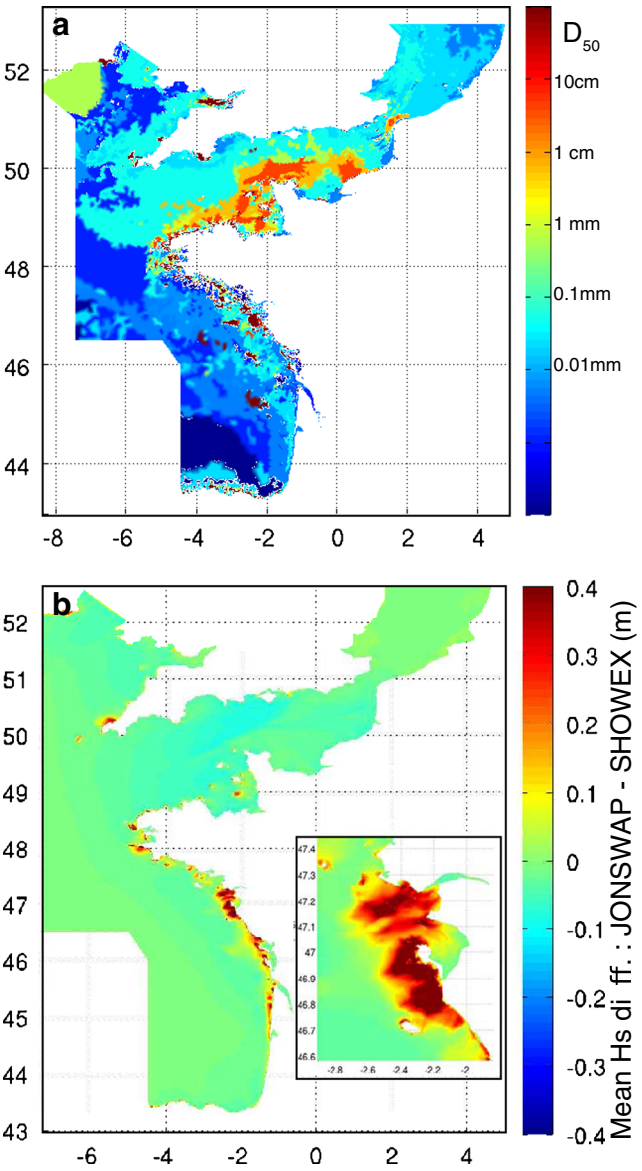

Fig. 6 **a** Map of sediment median diameter and **b** mean difference in significant wave height (in meters) over the month of February 2010 between a model run using the "JONSWAP" bottom friction parameterization and another using the "SHOWEX" parameterization with a constant Nikuradse roughness length of 12 cm for rocks. *Inset is* a zoom on the region around Yeu and Noirmoutier islands where the impact of this friction is very clear, as also shown in Fig. 7a

We have thus taken into account bottom types, particularly sand, gravel, and rocks. We started from the SHOWEX parameterization for movable beds, with which WW3 was verified to reproduce the ray-tracing results obtained by Ardhuin et al. (2003a) for the North Carolina Shelf. The parameterization was modified to give a constant Nikuradse roughness for rock bottoms. This roughness value was tuned here to 12 cm in order to reproduce the observed wave heights. This value was applied to all rocky areas. This modified bottom friction has limited impact at other locations

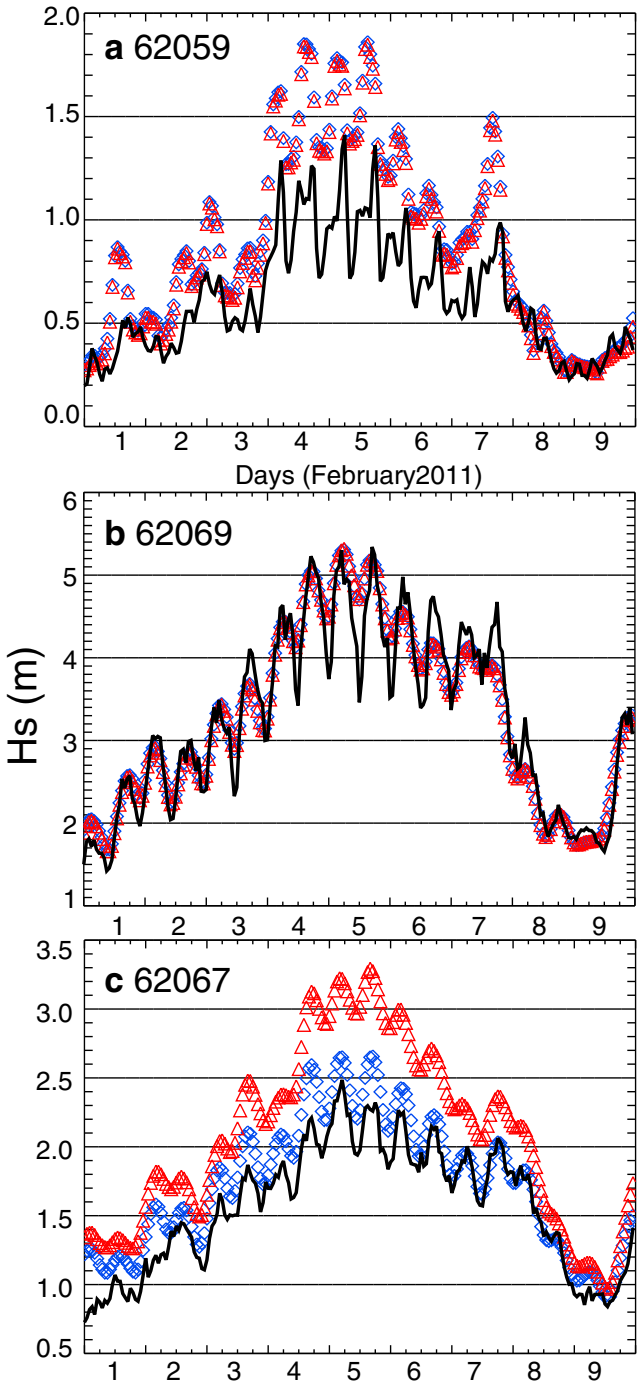

Fig. 7 Time series of observed and modeled significant wave height at several buoys using the JONSWAP (*blue diamonds*) or SHOWEX (*red triangles*) parameterizations for bottom friction, compared to hourly buoy measurements (*solid line*)

(Fig. 7, and Table 1). Such a large roughness value was also found to improve model results for waves crossing the rocky platform to the west of Sein island (not shown). Overall, the SHOWEX bottom friction yields lower wave heights in very shallow water and results that are quite close to the JONSWAP results in intermediate water depths.

Table 1 Statistics of model errors for the significant wave height H_s against buoy data for the NORGASUG model grid for the months of February and March 2011, using either the JONSWAP (BT1) or SHOWEX (BT4) parameterizations for bottom friction

Buoy	Longitude	Latitude	BT1, S.I.	BT1, N.B.	BT4, S.I.	BT4 N.B.
Four	−2.78	47.24	14.4	5.91	13.9	5.03
62064	−1.45	44.65	11.4	3.2	11.3	4.0
62066	−1.61	43.53	18.6	−6.5	18.2	−5.0
62067	−2.29	46.83	22.2	25.3	8.9	6.8
62069	−4.9	48.28	11.3	1.3	11.4	1.0
62059	−1.62	49.70	19.0	23.7	17.3	23.6
62072	1.37	50.66	24.4	4.1	25.0	0.5
62074	−3.3	47.3	10.8	−1.7	10.8	−2.1
62288	0.75	50.75	18.2	1.9	18.1	1.2

S.I. stands for scatter index, while N.B. is the bias normalized by the RMS observed value. Both are given in percent.

Table 1 shows that differences between the JONSWAP and SHOWEX parameterizations are significant only at buoys 62067 and 62059. Other buoys are generally in deeper water or exposed to relatively shorter wave periods for which bottom friction is not so important. This table also reveals that errors with the SHOWEX parameterization are largest at buoys 62072, located only 2 km from the breakwaters that protect the harbor of Cherbourg. At that location the maximum tidal range is 7 m. Currents as large as 1.5 m could be causing problems with the performance of the Datawell buoy, but the spectra look reasonable even during spring tides. Instead, it is likely that current gradients may not be well resolved in the tidal model or that their effect is not well represented in the wave model, unlike what was found for the region around buoy 62069 (Ardhuin et al. 2012). All these buoy results are consistent with the differences between model and altimeter data (Fig. 8), which are very useful for identifying regions with particular problems. For example, the North Sea suffers from a low bias which comes from the general short fetch bias in the chosen parameterization and, possibly, an exaggerated bottom friction. This area will require further attention.

Effect of coastal reflection In the Eastern Channel at buoy 62288 (Hastings) and 62072 (Vergoyer), waves are too short to be significantly modified by bottom friction, and the wave heights are generally underestimated by a few percent. This error may be largely due to an underestimation of waves at short fetch with the wind-wave growth parameterization of Ardhuin et al. (2010). At that site, however, we have found a beneficial impact of adding reflection off the shoreline, taking a uniform shoreface slope of 30 % to account for the steep beaches and cliffs and using the parameterization by Ardhuin and Roland (2012). Compared to our baseline

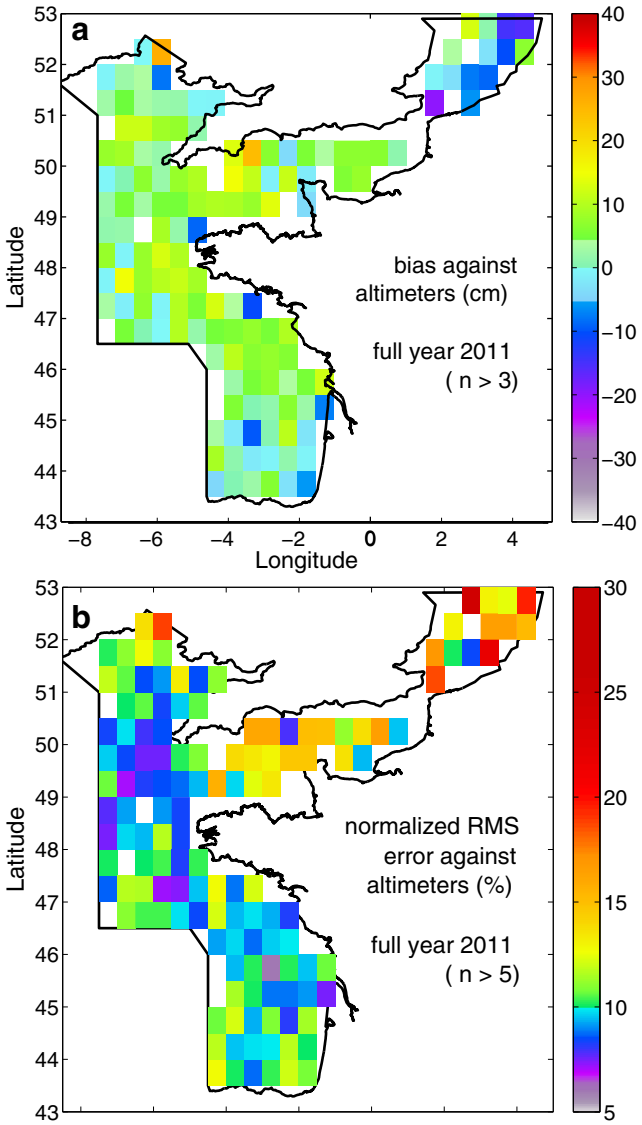

Fig. 8 Validation of the Bay of Biscay model grid for year 2011 using all available altimeter data. **a** Bias in centimeters and **b** normalized root mean square error (NRMSE). The satellite data was taken from the calibrated Ifremer database (Queffeulou 2010). The along-track time series at 1 Hz sampling was averaged over 0.5° along the track. These "super-observations" (SO) were then binned with latitude and longitude, with an average number of 35 SOs for 1 year in each 0.5 by 0.5° bin. Results are only shown for bins with at least four SOs for the bias and six SOs for the NRMSE

model run, the bias on wave heights was changed from 0.5 to 2.5 %. The directional properties were also improved by this added reflection, especially for the higher frequency range (0.15 to 0.4 Hz) with a significant reduction of the r.m.s. error on the mean direction, from 47 to 42°, and a strong reduction the bias and scatter index for the directional spread. These results are consistent with the model improvements reported for the US West Coast by Ardhuin and Roland (2012). We are waiting to assemble a database of shoreline slopes in order to implement this parameterization in our routine hindcasts and forecasts. This was done for most of the US West Coast using 1-m resolution lidar data. Data with such an extensive coverage are not yet available in Europe.

4 Summary and perspectives

Numerical wave models have evolved dramatically over the last two decades. Their accuracy has increased thanks to improvements in forcing fields and parameterizations, and they are now more capable of handling complex coastal topographies with numerical schemes that are efficient on small computer cluster or massively parallel machines.

A landmark in this progress will certainly be the version 4.18 of the WAVEWATCH III code now available from the National Centers for Environmental Prediction (NOAA/NCEP). This wave modeling framework has been augmented with many features, including improved parameterizations of wave generation and dissipation, bottom friction, and coastal reflection. The new code handles curvilinear, sperical multiple cell grids, and triangle-based meshes (e.g., Ardhuin et al. 2012). The latter type of grid has been thoroughly tested with 20-year hindcasts and routine forecasts. Here, we have used the explicit N-scheme on triangle meshes because it is faster than higher-order explicit schemes, and its larger diffusion gives weaker discretization effects known as the "garden sprinkler effect." This explicit scheme also gives smaller errors than its implicit version. The four different schemes for unstructured grids are available to users. There are trade-offs between model accuracy and its computational cost in the choice of numerical scheme or the choice between fractional step (splitting) methods and non-splitting methods. As for the cost, in our North Sea-Channel-Biscay mesh the spatial advection with the N-scheme only accounts for 22 % of the total computation cost. By allowing to put more nodes where there are gradients in the wave field, the irregular grids allow a much faster simulation than a regular grids with high resolution everywhere and that efficiency mostly come from the reduction in the number of nodes and thus in the time needed to compute source terms.

In WAVEWATCH III, the different grid types can be two-way nested in a single multigrid system. The code also allows coupling using generic couplers (Bennis 2011), or off-line forcing with all the necessary two- or three-dimensional fields. Many new applications are made possible by the greater accuracy of the shape of the wave spectrum, from remote sensing to seismology, and these new applications are providing error estimates that will in turn allow to refine the source term parameterizations (Rascle and Ardhuin 2013; Ardhuin et al. 2013).

Beyond the wave model itself, the basic numerical tools needed to investigate complex wave-current interaction problems are now available. The first benefit of these efforts will certainly be an improved wind and current forcing for the wave models, opening many exciting perspectives. From air-sea fluxes to sediment transport and the interpretation of remote sensing data, many applications can be found. Yet, the numerical schemes that are used up to know on unstructured meshes need further developments in order to be efficient and accurate in the nearshore, at resolutions smaller than 100 m, especially when coupled with circulation models.

Acknowledgments This work was made possible by the help and dedication of many, including J. Lepesqueur who generated the bottom type files and performed the initial simulations with variable roughness. All altimeter data processed by P. Queffeulou was kindly provided by CNES, ESA, and NOAA. We thank CETMEF, CEFAS, and SHOM for providing the buoy data and the organizers of Coastal Dynamics 2013 for soliciting this contribution. A.R. is funded by SHOM; F.A. is funded by ERC grant #240009 "IOWAGA" with additional support from the US National Ocean Partnership Program, under grant N00014-10-1-0383 and Labex Mer via grant ANR-10-LABX-19-01. A. Sepulveda kindly gave feedback on the manuscript draft.

References

Alves JHGM, Chawla A, Tolman HL, Schwab D, Lang G, Mann G (2013) The operational implementation of a great lakes wave forecasting system at NOAA/NCEP. Weather and Forecasting 28 (in press)

Andrews DG, McIntyre ME (1978) On wave action and its relatives. J Fluid Mech 89:647–664. corrigendum: vol. 95, p. 796

Ardhuin F, Herbers THC (2005) Numerical and physical diffusion: can wave prediction models resolve directional spread? J Atmos Ocean Technol 22(7):886–895

Ardhuin F, Herbers THC (2013) Double-frequency noise generation by surface gravity waves in finite depth: gravity, acoustic and seismic modes. J Fluid Mech 716:316–348

Ardhuin F, Magne R (2007) Current effects on scattering of surface gravity waves by bottom topography. J Fluid Mech 576:235–264

Ardhuin F, Roland A (2012) Coastal wave reflection, directional spreading, and seismo-acoustic noise sources. J Geophys Res 117:C00J20. doi:10.1029/2011JC007832

Ardhuin F, Roland A (2013) Spectral wave models, coastal and coupled aspects. In: Bonneton P, Garlan T (eds) Coastal Dynamics '13, University of Bordeaux, pp 25–38

Ardhuin F, Herbers THC, O'Reilly WC (2001) A hybrid Eulerian-Lagrangian model for spectral wave evolution with application to bottom friction on the continental shelf. J Phys Oceanogr 31(6):1498–1516

Ardhuin F, Herbers THC, Jessen PF, O'Reilly WC (2003a) Swell transformation across the continental shelf. Part II: validation of a pectral energy balance equation. J Phys Oceanogr 33:1940–1953

Ardhuin F, O'Reilly WC, Herbers THC, Jessen PF (2003b) Swell transformation across the continental shelf. Part I: Attenuation anddirectional broadening. J Phys Oceanogr 33:1921–1939

Ardhuin F, Rogers E, Babanin A, Filipot JF, Magne R, Roland A, van der Westhuysen A, Queffeulou P, Lefevre JM, Aouf L, Collard F (2010) Semi-empirical dissipation source functions for wind-wave models: part I, definition, calibration and validation. J Phys Oceanogr 40(9):1917–1941

Ardhuin F, Tournadre J, Queffelou P, Girard-Ardhuin F (2011) Observation and parameterization of small icebergs: drifting breakwaters in the southern ocean. Ocean Model 39:405–410

Ardhuin F, Dumas F, Bennis A-C, Roland A, Sentchev A, Forget P, Wolf J, Girard F, Osuna P, Benoit M (2012) Numerical wave modeling in conditions with strong currents: dissipation, refraction and relative wind. J Phys Oceanogr 42:2101–2120

Ardhuin F, Lavanant T, Obrebski M, Marié L, Royer JY, d'Eu JF, Howe BM, Lukas R, Aucan J (2013) A numerical model for ocean ultra low frequency noise: wave-generated acoustic-gravity and Rayleigh modes. J Acoust Soc Amer 134(4):3242–3259.

Becq-Girard F (1999) Non-linear propagation of unidirectional wave fields over varying topography. Coastal Eng 38:91–113

Benetazzo A (2006) Measurements of short water waves using stereo matched image sequences. Coastal Eng 53:1013–1032

Bennis AC (2011) On the coupling of wave and three-dimensional circulation models: choice of theoretical framework practical implementation and adiabatic tests. Ocean Model 40:260–272

Benoit M (1996) Development of a third generation shallow-water wave model with unstructured spatial meshing. In: Proceedings of the 25th International Conference on Coastal Engineering Marcos, F. ASCE, Orlando, pp 465–478

Bidlot J (2005) A revised formulation for ocean wave dissipation in CY25R1 Tech. Rep. Memorandum R60.9/JB/0516, Research Department, ECMWF, Reading, UK, Abdalla, S

Booij N, Holthuijsen LH (1987) Propagation of ocean waves in discrete spectral wave models. J Comp Phys 68:307–326

Booij N (1999) A third-generation wave model for coastal regions. 1. model description and validation, vol 104, Holthuijsen, LH, pp 7,649–7,666

Boudière E, Maisondieu C, Ardhuin F, Accensi M, Pineau-Guillou L, Lepesqueur J (2013) A suitable metocean hindcast database for the design of marine energy converters. Int J Mar Energy 28:e40–e52

Bouws E, Komen GJ (1983) On the balance between growth and dissipation in an extreme depth-limited wind-sea in the southern North Sea. J Phys Oceanogr 13:1653–1658

Cavaleri L, Bertotti L (1997) In search of the correct wind and wave fields in a minor basin. Mon Weather Rev 125(8):1964–1975

Csík Á, Ricchiuto M, Deconinck H (2002) A conservative formulation of the multidimensional upwind residual distribution schemes for general nonlinear conservation laws. J Comp Phys 172(2):286–312

Dietrich JC, Westerink JJ, Kennedy AB, Smith JM, Jensen RE, Zijlema M, Holthuijsen LH, Dawson C, Luettich RAJr, Powell MD, Cardone VJ, Cox AT, Stone GW, Pourtaheri H, Hope ME, Tanaka S, Westerink LG, Westerink HJ, Cobell Z (2011) Hurricane Gustav (2008) waves and storm surge: hindcast, synoptic analysis, and validation in southern Louisiana. Mon Weather Rev 139:2488–2522

Dietrich JC, Zijlema M, Allier PE, Holthuijsen LH, Booij N, Meixner JD, Proft JK, Dawson CN, Bender CJ, Naimaster A, Smith JM, Westerink JJ (2013) Limiters for spectral propagation velocities in SWAN. Ocean Model 139:85–102. doi:10.1016/j.ocemod.2012.11.005

Dommermuth D, Yue D (1987) A high-order spectral method for the study of nonlinear gravity waves. J Fluid Mech 184:267–288

Elfouhaily T, Thompson D, Vandemark D, Chapron B (1999) Weakly nonlinear theory and sea state bias estimations. J Geophys Res 104(C4):7641–7647

Farrell WE, Munk W (2008) What do deep sea pressure fluctuations tell about short surface waves? Geophys Res Lett 35(7):L19, 605. doi:10.1029/2008GL035008

Filipot JF, Ardhuin F (2012) A unified spectral parameterization for wave breaking: from the deep ocean to the surf zone. J Geophys Res 117:C00J08. doi:10.1029/2011JC007784

Garlan T (1995) La cartographie des sédiments du littoral français résultats et objectifs. J Rech Océanogr 20:50–54

Garlan T (2009) De la classification des sédiments à la cartographie de la nature des fonds marins. Ann Hydrogr 20:50–54

Godunov SK (1954) Different methods for shock waves, PhD thesis, Moscow State University

Gonzalez-Lopez JO, Westerink J, Mercado A, Capella J, Morell J, Canals M (2011) Effect of a steep and complex-featured shelf on computed wave spectra. In: Proceedings 12th international workshop of wave hindcasting and forecasting, Hawaii

Hanafin J, Quilfen Y, Ardhuin F, Vandemark D, Chapron B, Feng H, Sienkiewicz J, Queffeulou P, Obrebski M, Chapron B, Reul N, Collard F, Cormand D, de Azevedo EB, Vandemark D, Stutzmann E (2012) Phenomenal sea states and swell radiation: a comprehensive analysis of the 12–16 February 2011 North Atlantic storms. Bull Amer Meterol Soc 93:1825–1832

Hargreaves JC, Annan JD (2000) Comments on "Improvement of the short-fetch behavior in the wave ocean model (WAM)". J Atmos Ocean Technol 18:711–715

Hasselmann K, Barnett TP, Bouwsm E, Carlson H, Cartwright DE, Enke K, Ewing JA, Gienapp H, Hasselmann DE, Kruseman P, Meerburg A, Müller P, Olbers DJ, Richter K, Sell W, Walden H (1973) Measurements of wind-wave growth and swell decay during the Joint North Sea Wave Project. Deut Hydrogr Z 8(12):1–95. suppl. A

Herbers THC, Burton MC (1997) Nonlinear shoaling of directionally spread waves on a beach. J Geophys Res 102(C9):21,101–21,114

Hersbach H, Janssen PAEM (1999) Improvement of the short-fetch behavior in the wave ocean model (WAM). J Atmos Ocean Technol 16:884–892

Holthuijsen LH, Herman A, Booij N (2003) Phase-decoupled refraction-diffraction for spectral wave models. Coastal Eng 49:291–305

Janssen PAEM (2008) Progress in ocean wave forecasting. J Comp Phys 227:3572–3594. doi:10.1016/j.jcp.2007.04.029

Janssen PAEM (2009) On some consequences of the canonical transformation in the Hamiltonian theory of water waves. J Fluid Mech 637:1–44

Komen GJ, Cavaleri L, Donelan M, Hasselmann K, Hasselmann S, Janssen PAEM (1994) Dynamics and modelling of ocean waves. Cambridge University Press, Cambridge

de Laplace PS (1776) Suite des recherches sur plusieurs points du système du monde (XXV–XXVII), Mém Présentés Acad R Sci Inst France, pp. 542-552

Lax PD, Richtmyer RD (1956) Survey of the stability of linear finite difference equations. Comm Pure Appl Math 9:267–293

Leonard BP (1991) The ULTIMATE conservative difference scheme applied to unsteady one-dimensional advection. Comput Methods Appl Mech Eng 88:17–74

Li JG (2010) Global transport on a spherical multiple-cell grid. Mon Weather Rev 139:1536–1555. doi:10.1175/2010MWR3196.1

Liau JM, Roland A, Hsu TW, Ou SH, Li YT (2011) Wave refraction-diffraction effect in the wind wave model WWM. Coastal Eng 58:429–443

Magne R, Belibassakis K, Herbers THC, Ardhuin F, O'Reilly WC, Rey V (2007) Evolution of surface gravity waves over a submarine canyon. J Geophys Res 112:C01,002. doi:10.1029/2005JC003035

O'Reilly WC, Guza RT (1991) Comparison of spectral refraction and refraction-diffraction wave models. J Waterway Port Coast Ocean Eng 117(3):199–215

Patankar S (1980) Numerical heat transfer and fluid flow: computational methods in mechanics and thermal science. Hemisphere Publishing Corp., Washington

Phillips OM (1977) The dynamics of the upper ocean. Cambridge University Press, London, p 336

Popinet S, Gorman RM, Rickard GJ, Tolman HL (2010) A quadtree-adaptive spectral wave model, vol 34, pp 36–49

Priestley MB (1965) Evolutionary and non-stationary processes. J Roy Statist Soc Ser B 27:204–237

Queffeulou P (2010) Global altimeter SWH data set, version 7, Ifremer, France

Rascle N, Ardhuin F (2013) A global wave parameter database for geophysical applications. Part 2: model validation with improved source term parameterization. Ocean Modelling (in press)

Rascle N, Ardhuin F, Queffeulou P, Croizé-Fillon D (2008) A global wave parameter database for geophysical applications. Part 1: wave-current-turbulence interaction parameters for the open ocean based on traditional parameterizations, vol 25, pp 154–171

Rayevskiy MA (1983) On the propagation of gravity waves in randomly inhomogeneous nonsteady-state currents. Izv Atmos Ocean Phys 19(6):475–479

Ris R, Holthuijsen LH, Smith JM, Booij N, van Do ngeren AR (2002) The ONR virtual testbed for coastal and oceanic wave models. In: Proc. 28th Int. Conf. Coastal Engng., ASCE, Cardiff, ASCE, pp 380–391

Ris RC, Booij N, Holthuijsen LH (1999) A third-generation wave model for coastal regions. 2. Verification. J Geophys Res 104(C4):7,667–7,681

Rogers WE, Kaihatu JM, Petit HAH, Booij N, Holthuijsen LH (2002) Diffusion reduction in an arbitrary scale third generation wind wave model, vol 29, pp 1357–1390

Roland A (2008) Development of WWM II: spectral wave modelling on unstructured meshes. PhD thesis, Technische Universität Darmstadt, Institute of Hydraulic and Water Resources Engineering

Roland A, Zhang YJ, Wang HV, Meng Y, Teng YC, Maderich V, Brovchenko I, Dutour-Sikiric M, Zanke U (2012) A fully couple 3D wave-current interaction model on unstructured grids. J Geophys Res 117:C00J33. doi:10.1029/2012JC007952

Saha S, Moorthi S, Pan HL, Wu X, Wang J, Nadiga S, Tripp P, Kistler R, Woollen J, Behringer D, Liu H, Stokes D, Grumbine R, Gayno G, Wang J, Hou YT, ya Chuang H, Juang HMHaJS, Iredell M, Treadon R, Kleist D, Delst PV, Keyser D, Derber J, Ek M, Meng J, Wei H, Yang R, Lord S, van den Dool H, Kumar A, Wang W, Long C, Chelliah M, Xue Y, Huang B, Schemm JK, Ebisuzaki W, Lin R, Xie P, Chen M, Zhou S, Higgins W, Zou CZ, Liu Q, Chen Y, Han Y, Cucurull L, Reynolds RW, Rutledge G, Goldberg M (2010) The NCEP Climate Forecast System Reanalysis. Bull Amer Meterol Soc 91:1015–1057

Shemdin OH, Hsiao SV, Carlson HE, Hasselmann K, Schulze K (1980) Mechanisms of wave transformation in finite depth water. J Geophys Res 85(C9):5012–5018

SWAMP Group (1984) Ocean wave modelling. Plenum Press, New York

Tanaka M (2001) Verification of Hasselmann's energy transfer among surface gravity waves by direct numerical simulations of primitive equations. J Fluid Mech 444:199–221

Tayfun A (1980) Narrow-band nonlinear sea waves. J Geophys Res 85(C3):1543–1552

Fedele F, Tayfun A (2007) Wave height distributions and nonlinear effects. Ocean Eng 34:1631–1649

Thornton EB, Guza RT (1983) Transformation of wave height distribution. J Geophys Res 88(C10):5,925–5,938

Toledo Y, Hsu TW, Roland A (2012) Extended time-dependent mild-slope and wave-action equations for wave-bottom and wave-current interactions. Proc Roy Soc Lond A 468:184–205. doi:10.1098/rspa.2011.037

Tolman HL (1994) Wind waves and moveable-bed bottom friction. J Phys Oceanorg 24:994–1,009

Tolman HL (2002a) Alleviating the garden sprinkler effect in wind wave models. Ocean Model 4:269–289

Tolman HL (2002b) Distributed memory concepts in the wave model WAVEWATCH III. Parallel Comput 28:35–52

Tolman HL (2008) A mosaic approach to wind wave modeling. Ocean Model 25:35–47. doi:10.1016/j.ocemod.2008.06.005

Tolman HL (2009) User manual and system documentation of WAVEWATCH-III^{TM} version 3.14. Tech. Rep. 276, NOAA/NWS/NCEP/MMAB

Tolman HL, Chalikov D (1996) Source terms in a third-generation wind wave model. J Phys Oceanogr 26:2497–2518

Tolman HL, Banner ML, Kaihatu JM (2013) The NOPP operational wave model improvement project. Ocean Model 70:2–10. doi:10.1016/j.ocemod.2012.11.011

Touboul J, Rey V (2012) Bottom pressure distribution due to wave scattering near a submerged obstacle. J Fluid Mech 702:444–459

Vincent CL, Briggs MJ (1989) Refraction-diffraction of irregular waves over a mound. J Waterway Port Coast Ocean Eng 115:269–284

WAMDI Group (1988) The WAM model—a third generation ocean wave prediction model. J Phys Oceanogr 18:1775–1810

van der Westhuysen AJ, Zijlema M, Battjes JA (2007) Saturation-based whitecapping dissipation in SWAN for deep and shallow water. Coastal Eng 54:151–170

van der Westhuysen AJ, van Dongeren AR, Groeneweg J, van Vledder GP, Peters H, Gautier C, van Nieuwkoop JCC (2012) Improvement in spectral wave modelling in tidal inlet seas. J Geophys Res 117:C00J28

Willebrand J (1975) Energy transport in a nonlinear and inhomogeneous random gravity wave field. J Fluid Mech 70:113–126

Wingeart KM (2001) Validation of operational global wave prediction models with spectral buoy data. Master's thesis, Naval Postgraduate School, Monterey, CA

WISE Group (2007) Wave modelling—the state of the art. Prog Oceanogr 75:603–674. doi:10.1016/j.pocean.2007.05.005

Yanenko NN (1971) The method of fractional steps. Springer

Zijlema M, van der Westhuysen AJ (2005) On convergence behaviour and numerical accuracy in stationary SWAN simulations of nearshore wind wave spectra. Coastal Eng 53:237–256. doi:10.1016/j.coastaleng.2004.12.006

Zijlema M (2010) Computation of wind-wave spectra in coastal waters with SWAN on unstructured grids. Coastal Eng 57:267–277